Quantum dot strain engineering of InAs/InGaAs nanostructures

L. Seravalli,[a] M. Minelli, P. Frigeri, and S. Franchi
CNR-IMEM, Parco delle Scienze 37a, I-43100 Parma, Italy

G. Guizzetti, M. Patrini, and T. Ciabattoni
CNISM-Dipartimento di Fisica "A. Volta," Università degli Studi di Pavia, Via Bassi 6, I-27100 Pavia, Italy

M. Geddo
CNISM-Dipartimento di Fisica, Università degli Studi di Parma, Viale delle Scienze 7a, I-43100 Parma, Italy

(Received 15 May 2006; accepted 7 November 2006; published online 19 January 2007)

We present a complete study both by experiments and by model calculations of quantum dot strain engineering, by which a few optical properties of quantum dot nanostructures can be tailored using the strain of quantum dots as a parameter. This approach can be used to redshift beyond 1.31 μm and, possibly, towards 1.55 μm the room-temperature light emission of InAs quantum dots embedded in InGaAs confining layers grown on GaAs substrates. We show that by controlling simultaneously the lower confining layer thickness and the confining layers' composition, the energy gap of the quantum dot material and the band discontinuities in the quantum dot nanostructure can be predetermined and then the light emission can be tuned in the spectral region of interest. The availability of two degrees of freedom allows for the control of two parameters, which are the emission energy and the emission efficiency at room temperature. The InAs/InGaAs structures were grown by the combined use of molecular beam epitaxy and atomic layer molecular beam epitaxy; their properties were studied by photoluminescence and photoreflectance spectroscopies and by atomic force microscopy; in particular, by means of photoreflectance not only the spectral features related to quantum dots were studied but also those of confining and wetting layers. The proposed approach has been used to redshift the room-temperature light emission wavelength up to 1.44 μm. The optical results were analyzed by a simple effective-mass model that also offers a rationale for engineering the properties of structures for efficient long-wavelength operation. © *2007 American Institute of Physics*. [DOI: 10.1063/1.2424523]

I. INTRODUCTION

Quantum dots (QDs) are semiconductor nanostructures based on three-dimensional self-assembled islands embedded in layers of semiconductor materials with larger energy gap and suitable band discontinuities, where zero-dimensional systems of carriers can be achieved.[1] The most studied systems are unarguably those based on the InAs/GaAs one, due to the possibility of obtaining QD light emission in the spectral window of optical fiber communications at 1.31 μm and, eventually, at 1.55 μm by using structures grown on GaAs substrates, much more advantageous than those deposited on InP.[2]

As the QD emission energy depends in a complex way on several parameters, both related to the growth conditions and to the structure design, a considerable amount of research work has been done in these last years to achieve the redshift of the QD emission necessary to extend device operation to 1.55 μm. Many different methods have been proposed and implemented, which can be categorized into three main approaches: (i) the increase of QD dimensions, (ii) the change in the band discontinuity between QDs and confining layers (CLs), and (iii) the reduction of the energy gap of the QD material.

In the first approach the increase of QD dimensions has been obtained by acting on molecular beam epitaxy (MBE) growth parameters by (a) reducing the InAs growth rate,[3,4] (b) using alternative MBE technique such as atomic layer molecular beam epitaxy (ALMBE),[5] and (c) using other alternating-beam techniques.[6,7]

The second approach has been the most widely adopted so far, as the insertion of InGaAs confining layers below and/or above the QDs allowed many groups to tune the emission wavelength at 1.31 μm at room temperature.[8–12] Due to the reduced lattice mismatch to InAs QDs, InGaAs CLs cause also a reduction of the QD strain, that therefore contributes to the redshift of the QD light emission. Furthermore, some authors invoked yet another effect to explain the redshift of InAs QD emission energy when embedding QDs with InGaAs layers, namely, the increased QD dimensions and/or the changed QD composition due to strain-driven In migration from InGaAs upper confining layers to QDs.[8,13]

Finally, approach (iii) has been proven to be very useful in reaching emission at 1.55 μm by growing In(Ga)As QDs on either metamorphic buffers on GaAs (Refs. 14–16) or directly on InP,[17] thus reducing the QD strain and decreasing the QD energy gap. These considerations show that a com-

[a]Electronic mail: seravall@imem.cnr.it

prehensive understanding of the effects of all design and growth parameters—a necessary step towards the engineering of such nanostructures—is still lacking.

In a previous work[14] it was shown that the redshift of emission from InAs/InGaAs QD structures can be achieved both by increasing the In composition in the InGaAs CLs and by decreasing the QD strain. In particular, the QD strain was reduced by controlling the QD-CL mismatch, which depends on the lattice parameter a_{LCL} of the lower confining layer (LCL) for any given QD composition; a_{LCL}, in turn, is determined, at any given composition, by the thickness-dependent strain relaxation of LCL; in conclusion, the authors were able to demonstrate that the band discontinuities of InAs/InGaAs QD structures and the strain of QDs (and consequently their energy gap) can be chosen by acting on two independent parameters that are the CL composition and the LCL thickness.

The redshift was experimentally evidenced by means of photoluminescence[14] (PL) and photoreflectance (PR) spectroscopies.[18] Photoreflectance measurements also confirmed the possibility of determining the extent of strain relaxation of LCLs as a function of their thickness.[19]

These experimental results suggested the concept of *QD strain engineering* (i.e., the possibility of engineering a few optical properties of QDs by controlling their strain status), that was also supported by a simple effective-mass model of electronic fundamental transitions in InAs/InGaAs QD structures.[14] In addition, it was also shown that by using such an approach, the room-temperature (RT) efficiency of luminescence can be optimized while keeping the emission at a predetermined wavelength.[20]

In this paper we systematically study by means of photoluminescence and photoreflectance the implications of QD strain engineering and show how the model previously developed can be effectively used to engineer the structures and to understand their light emission properties. The experimental results show that the strain engineering realized in our structures is in a very satisfactory agreement with the predictions and that it can be used as a valuable tool to extend the operation wavelength of light-emitting devices towards 1.55 μm.

In Sec. II we present experimental details on the MBE preparation of the structures, PL and PR spectroscopies, and atomic force microscopy (AFM), on the PR data reduction procedure and analysis, on the model used to study the emission energy of the QD structures, and finally, on the developed approach to control the strain of QDs by using metamorphic buffers. Sections III A and III B deal with the experimental results and their discussion relative to QD and CL transitions. The approach of QD strain engineering is thoroughly discussed in Sec. III C; finally, in Sec. III D, by using both model calculations and experimental data, we present the possibility of enhancing the PL efficiency at RT by increasing the energy barriers that confine the carriers into the QDs while keeping the emission wavelengths at the intended values. Conclusions are presented in Sec. IV.

II. EXPERIMENTAL, ANALYSIS, AND MODEL DETAILS

A. Experimental and data analysis

The structures considered in this work were grown by MBE on semi-insulating (100) GaAs substrates. On top of a 100 nm thick GaAs buffer layer, we deposited at 490 °C the $In_xGa_{1-x}As$ metamorphic LCL with In molar fraction x (hereafter termed as composition x) and thickness t. After a growth interruption of 210 s to lower the substrate temperature, we grew by ALMBE (Ref. 21) at 460 °C the InAs QDs with a 3.0 ML (monolayer) coverage and capped them with a 20 nm thick InGaAs upper confining layer (UCL) with the same composition as the LCL and deposited by ALMBE at 360 °C.[5] Uncapped structures for AFM characterization were grown under the same conditions.

Continuous-wave PL was performed in the 10–300 K temperature range: the excitation source was the 532 nm laser line, with a power density of about 5 W/cm^2. The PL spectra were measured by a fast-Fourier transform spectrometer with a 1 meV resolution and a cooled Ge detector.

PR measurements in the 80–300 K temperature range were performed at near-normal incidence in the 0.7–1.6 eV range, with energy step and spectral resolution of 1 meV. The modulation source was provided by a 16 mW He–Ne laser, mechanically chopped at a frequency of 220 Hz. Further details are reported elsewhere.[18,19] The analysis of the PR spectra was carried out by using typical line shape models characterizing electromodulated signals in semiconductor systems, following the treatment suggested by Aspnes,[22] who showed that near a critical point (CP) the line shape may be expressed by

$$\Delta R/R = \mathrm{Re}[Ce^{i\varphi}(E - E_{CP} + i\Gamma)^{-n}], \quad (1)$$

where E is the energy of the probe beam, C and φ are an amplitude and a phase factor that vary slowly with E, E_{CP} is the CP energy, and Γ is the (Lorentzian) broadening parameter; to interpret the PR spectral features we used $n=2.5$ to reproduce bulk band-to-band transitions[22] and $n=3$ to reproduce quantum-confined exciton transitions.[23–28]

AFM measurements of structures without UCLs were carried out in contact-mode configuration. By taking into account the QD-tip convolution effects, QD height and diameter distributions were extracted by topographic images.

B. Quantum dot strain engineering and modeling of QD electronic transitions

As discussed in Sec. I, the strain of QDs induced by the confining layers was considered as a factor determining the QD emission energy since the work of Ref. 9. Seravalli *et al.*[14] showed that the QD strain and then the energy of electronic transitions can be controlled not only by the CL composition but also by taking advantage of the thickness-dependent strain relaxation of mismatched LCLs, that act as metamorphic buffers.[19] Due to this mechanism the lattice parameter of an InGaAs LCL grown on GaAs equals that of GaAs in the pseudomorphic regime, that is, for thicknesses smaller than the so-called critical thickness t_c for strain re-

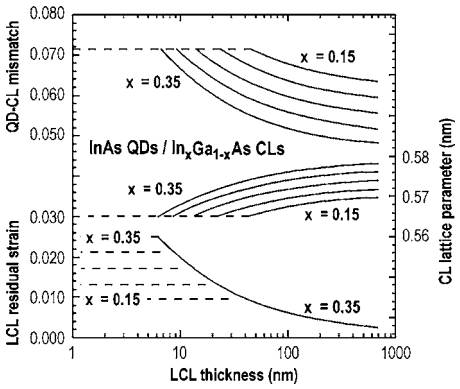

FIG. 1. Dependences of residual strain in LCL, CL lattice parameter, and QD-CL lattice mismatch on LCL thickness in InAs/In$_x$Ga$_{1-x}$As structures in the pseudomorphic (dashed lines) and metamorphic (continuous lines) regimes. The strain relaxation in LCLs has been calculated according to the model of Marée *et al.* (Ref. 29).

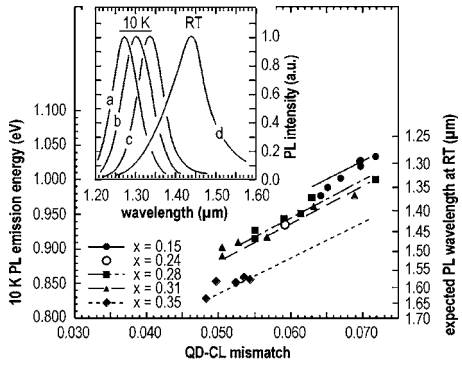

FIG. 2. 10 K PL emission energy and expected RT emission wavelength as functions of QD-CL mismatch in InAs/In$_x$Ga$_{1-x}$As QD strain-engineered nanostructures with In composition x. The lines represent the results of the model calculations. In the inset are shown 10 K PL emission spectra of structures with $x=0.28$ and $f=0.0630$ (a), $f=0.0614$ (b), and $f=0.0550$ (c) and the PL emission spectrum at RT of the structure with $x=0.24$ and $f=0.0592$, peaked at 1.44 μm. This structure is represented in the main plot by the open circle.

laxation, whereas it increases up to that of freestanding InGaAs with the composition x for increasing thickness, thus reducing the QD-LCL mismatch.

The calculation of the QD-LCL mismatch $f=(a_{\mathrm{InAs}}-a_{\mathrm{LCL}})/a_{\mathrm{LCL}}$ (where a_{LCL} and a_{InAs} are the lattice parameters of the partially relaxed InGaAs LCL and of freestanding unstrained InAs, respectively) as a function of the In molar fraction x and thickness t of the InGaAs LCLs was carried out following the nonequilibrium model for strain relaxation of Marée *et al.*[29] The parameter a_{LCL} is related to the in-plane residual strain $\varepsilon=(a_{\mathrm{InGaAs}}-a_{\mathrm{LCL}})/a_{\mathrm{LCL}}$ that, in turn, can be approximated by $\varepsilon=\varepsilon_0(t_c/t)^{1/2}$, where $\varepsilon_0=(a_{\mathrm{InGaAs}}-a_{\mathrm{GaAs}})/a_{\mathrm{GaAs}}$ is the strain of InGaAs pseudomorphic layer grown on (001) GaAs substrates;[29] in the above equations, a_{InGaAs} and a_{GaAs} are the lattice parameters of unstrained, freestanding InGaAs and GaAs, respectively. As for the UCLs, we consider them as pseudomorphic to the LCLs and then having the same lattice parameter as LCLs; this assumption is confirmed by the PR results that will be discussed in Sec. III B; hereafter the lattice parameter of CLs will be denoted by a_{CL}.

In Fig. 1, the LCL residual strain ε, the LCL lattice parameter a_{CL}, and the QD-CL mismatch f are shown as functions of t for different values of x. In Ref. 19, it was discussed thoroughly that the predictions of Marée *et al.*[29] agree with the PR determination of ε in a much more satisfactory extent than those of equilibrium models,[30,31] that foresee a $\varepsilon \propto t^{-1}$ strain dependence.

To analyze the dependence of QD ground-state emission energy on x and f, we developed a simple model based on a single-band, effective-mass approach for QDs with cylindrical symmetry, following the work of Marzin and Bastard.[32] While other more complex models have been presented in the literature in these last years, such as the ones based on pseudopotential treatment,[33] effective-mass approach for pyramidal QDs,[34] and $\mathbf{k}\cdot\mathbf{p}$ methods with four and eight band,[35,36] it has been shown that the effective-mass approximation can be considered satisfying when only ground-state calculation is needed, as in our case.[36,37] We considered QDs with truncated conical shapes and with base diameters and heights given by the most frequent values in the respective distributions derived by AFM characterization; values of the ratio between base and top diameters were taken similar to those reported in the literature (2.5–3.0).[38,39] In order to calculate the QD strain, we followed the analytical approach of Andreev *et al.*,[40] where values for the hydrostatic and biaxial components in InAs QDs embedded in GaAs are given as linear functions of the QD-CL mismatch. The band discontinuities between QDs and CLs were derived from the model solid theory (MST),[41] that takes strain effects into account. The MST parameters of InGaAs were deduced from those of the binary constituents as proposed by Cardona and Christensen.[42]

III. RESULTS AND DISCUSSION

A. Electronic transitions related to QD states

In the main plot of Fig. 2 we show the PL emission energy at 10 K (symbols) of InAs/InGaAs QD structures as a function of the mismatch f between QDs and CLs for different compositions of CLs, alongside model calculations (lines). The values of f have been calculated with the procedure outlined in Sec. II B and illustrated in Fig. 1, on the basis of the model of Marée *et al.* for the strain relaxation of the LCLs.[29] As shown in Sec. III B the residual strain values calculated according to Ref. 29 compare very favorably with that obtained by PR measurements on the strain-induced top valence band splitting in CLs. The parameter values adopted in the model such as the electronic band structure ones and the elastic constants of materials were all taken from the literature[43,14] and not trimmed to fit the experimental data. In the inset of Fig. 2 we present PL spectra at 10 K for structures with composition $x=0.28$ and mismatches $f=0.0630$, 0.0614, and 0.0550 to highlight the effect of the mismatch reduction on the QD emission and also the PL spectrum at RT for the structure ($x=0.24$ and $f=0.0592$) that showed the longest emission wavelength (1.44 μm) at RT under low (5 W/cm^2) excitation power density. This structure is represented in the main plot by the open circle. In order to discuss the redshift of transition energies at RT even in structures

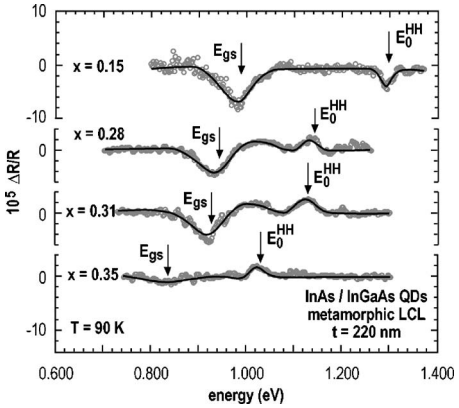

FIG. 3. PR spectra at 90 K of InAs/$In_xGa_{1-x}As$ nanostructures with LCL of thickness t=220 nm and different compositions x highlighting the simultaneous detection of the signal coming from QDs (E_{gs}) and CLs (E_0^{HH}). Arrows mark the transition energies as obtained from the best fit (solid lines) of the experimental line shape (circles).

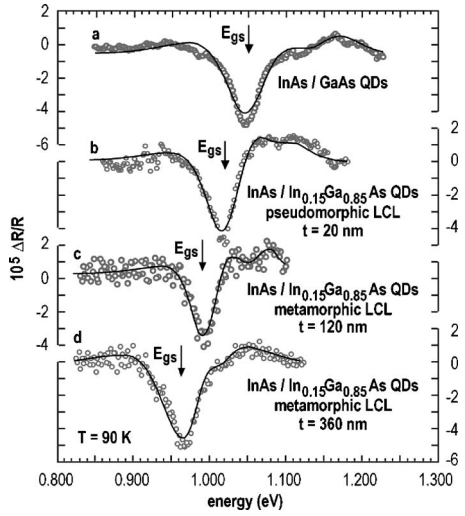

FIG. 4. PR spectra at 90 K of InAs QD ground-state transition E_{gs} for an InAs/GaAs structure (a) and for InAs/$In_{0.15}Ga_{0.85}As$ structures with LCL thicknesses of 20 nm (b), 120 nm (c), and 360 nm (d). The redshift of (b) as compared to (a) and of (d) with respect to (c) are due to different band discontinuities and to different QD strains, respectively.

that do not emit at RT due to the thermal quenching of PL (Sec. III D), we converted the 10 K emission energy to the RT expected emission wavelength (right hand scale in Fig. 2) by considering a Varshni[44] shift of 70 meV, when increasing the temperature from 10 K to RT.

In the figure it can be noticed that the reduction of the mismatch (i.e., the decrease of the QD strain) causes a redshift of the QD emission energy for all compositions. On the other hand, for structures with the same QD-CL mismatch, the increase of the x value also leads to a reduction of the QD emission energy. As shown in Fig. 2, it is noticeable that the reduction of the QD strain would result in a redshift of emission to values in excess of the technologically important wavelength of 1.55 μm at RT, if the luminescence were not thermally quenched.

The agreement between model calculations and experimental results is quite satisfactory, the discrepancies being not larger than 25 meV, a value fully accounted for by uncertainties in QD sizes measured by AFM and by the approximations in the model and in its input parameters.

In Fig. 3, typical 90 K PR spectra are reported for structures with different CL compositions x and the same LCL thickness (t=220 nm). Taking advantage of the derivative-like nature of PR spectroscopy, signals due to even very weak spectral features were detected and unambiguously assigned to bulk- and QD-related transitions. The two PR features (labeled E_0^{HH} and E_{gs}) can be related for their energy position[45,46] to transitions involving the fundamental energy gap of the partially relaxed $In_xGa_{1-x}As$ CLs (Ref. 46) and the ground state of the InAs/InGaAs QDs (Ref. 14) of the main QD family,[28] respectively. Arrows mark the transition energies, as derived from the best fit of the optical spectra obtained by using the aforementioned line shape models, given by Eq. (1) with n=2.5 for CLs and n=3 for QD structures.

In Fig. 4, we present the 90 K PR spectra of InAs QDs embedded in GaAs CLs (a) alongside otherwise similar structures, but with $In_{0.15}Ga_{0.85}As$ CLs and different LCL thicknesses [20 nm (b), 120 nm (c), and 360 nm (d)]. AFM characterization of uncapped structures showed no change in QD sizes for this range of LCL composition and QD-LCL mismatch (see Sec. III C), therefore shifts in QD energy are due only to QD-CL band discontinuities and QD strain. The comparison of spectra (a) and (b) qualitatively shows the effect of CL composition on E_{gs}, since in both structures the strain field experienced by the QDs is the same; indeed, in the InAs/GaAs structure the LCL is lattice matched to the GaAs substrate, while in the InAs/InGaAs the LCL is pseudomorphic [$t<t_c$=43 nm (Ref. 29)] to the same substrate. Consequently, the redshift of the E_{gs} energy is only related to the reduction of band discontinuities. In the case of spectra (c) and (d), the redshift of the E_{gs} transition energy for the structure with thicker LCLs is due to the reduction of the QD strain, related to the lower mismatch of QDs to the CLs. The above results will be considered again in Sec. III C and represent a clear experimental confirmation of the predictions of QD strain engineering.

B. Electronic transitions related to CLs

An example of the ability of photoreflectance to detect at the same time transitions in both InAs wetting layers (WLs) and InGaAs CLs is shown in Fig. 5, where typical RT PR spectra for structures with x=0.15 and different LCL thicknesses ($t>t_c$=43 nm) are reported. The broad PR feature, in the low energy part of the spectra (E_{WL}) can be related to the wetting layer and will be discussed later on. The two PR features denoted as E_0^{HH} and E_0^{LH} have been previously attributed[19] to the interband transitions from the heavy-hole (HH) and the light-hole (LH) valence bands, split by the residual strain in LCLs.[47,48]

From the experimentally measured splitting $\Delta E=E_0^{LH}-E_0^{HH}$ the residual strain of the CLs can be deduced.[19] The values of the optically determined ε are in good agreement[19] with those of the model of strain relaxation of Marée *et al.*,[29] that was used to design the structures.

It is interesting to note that PR measurements performed on structures without UCLs showed negligible variations in

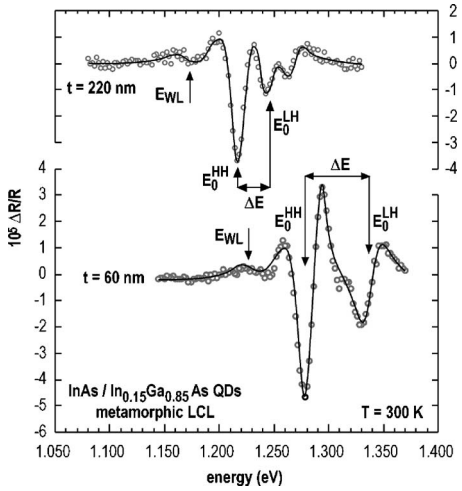

FIG. 5. RT PR spectra of $InAs/In_{0.15}Ga_{0.85}As$ structures with different LCL thicknesses. Evidence is given for the shift of the band gaps E_0^{HH} and E_0^{LH} and for their splitting $\Delta E=E_0^{LH}-E_0^{HH}$ as induced by the CL residual strain. The low energy PR feature, labeled E_{WL}, is due to the optical response of the wetting layer. Arrows mark the transition energies derived from the best fit (solid line) to the experimental line shape (open circles).

both broadening parameter and CP energy values of E_0^{HH} and E_0^{LH} transitions, suggesting that UCLs are pseudomorphic to LCLs and justifying *a posteriori* this assumption in the model for engineering the QD emission wavelength (Sec. II B).

In Fig. 6, the values of the CL fundamental energy gap for heavy holes E_0^{HH} are plotted as a function of the LCL thickness t for the structures with LCL composition $x=0.15$ and thickness ranging from 20 to 360 nm. In the same figure we reported the QD ground-state emission energies E_{gs} as measured both by PL (at 10 K) and by PR (at 90 K and shifted to 10 K by means of the Varshni law[44]) and model calculations for both the energy gap E_0^{QD} of the QD material and E_0^{HH}; in the figure inset these quantities are indicated in a

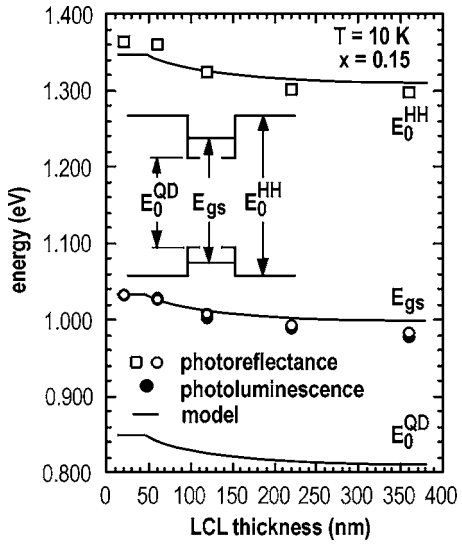

FIG. 6. Comparison of the behavior of QD ground-state transition E_{gs} vs LCL thickness, as obtained by PR and PL measurements (symbols) and by model calculations (line). The measured (symbols) and calculated (solid line) CL energy gap E_0^{HH} and the calculated energy gap E_0^{QD} of the QD material are also reported.

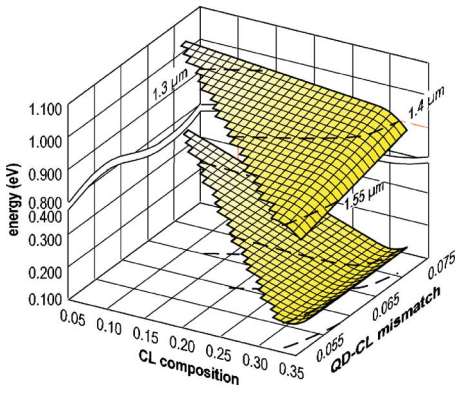

FIG. 7. (Color online) Calculated PL emission energy at 10 K (upper surface) and activation energy for the thermal escape of carriers from QDs to CLs (lower surface) as functions of the QD-CL mismatch f and the CL composition x in $InAs/In_xGa_{1-x}As$ QD strain-engineered nanostructures. The dashed lines represent the (x,f) pairs that result in RT emission at the indicated wavelengths.

schematic of the band structure along one arbitrary spatial direction. PR data of QD ground-state emission are very close to the PL ones and both satisfactorily follow the model predictions. Figure 6 clearly evidences that the QD energy redshift for increasing t and constant x is due to the reduction of the energy gap of the QD material, as caused by the decrease of the QD strain, while the sum of band discontinuities between QD and CLs, given by the difference between E_0^{HH} and E_0^{QD}, is very little affected by the LCL thickness determining the QD strain. This feature will be further discussed in the following section.

C. Quantum dot strain engineering

A rationale behind the experimental results shown so far can be found by using the results of our model (Sec. II B). In Fig. 7 the upper surface represents the calculated 10 K transition energy of InAs/InGaAs QD structures [including the effect of the exciton binding energy (20 meV) (Ref. 34)] reported as a function of the CL composition x and the QD-CL mismatch f. The three dashed lines on the (x,f) plane represent the calculated (x,f) pairs that result in 300 K emission at the 1.3, 1.4, and 1.5 μm wavelengths. The lines are also projected to the upper surfaces.

The sharp decrease of E_{gs} as x increases beyond 0.33 is related to the abrupt change of QD diameters that takes place at these values of x; as a consequence of the sudden increase in QD diameters, electron and hole quantum-confined levels deepen in the potential well. Indeed, while the AFM measured diameters are almost constant for $x\leqslant 0.33$ (21 ± 4 nm) they dramatically increase up to 29 ± 4 nm for $x=0.35$; on the contrary, the QD heights (4 ± 1 nm) are scarcely dependent on x and both diameters and heights are basically unaffected by the QD-CL mismatch f.

In Ref. 20 it has been shown that by using the results of our model (Fig. 7), different structures intended for 1.3, 1.4, and 1.5 μm emissions at RT can be engineered and prepared by MBE, with a good agreement between targeted and measured values of the operating wavelengths, thus giving a reasonable confidence in the use of the present implementation of the model.

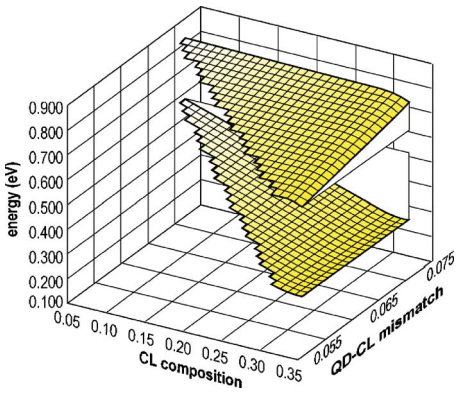

FIG. 8. (Color online) Calculated energy gap of the QD material (strained InAs) (upper surface) E_0^{QD} and sum of band discontinuities for electrons and holes (lower surface) as functions of the QD-CL mismatch and the CL composition x in $InAs/In_xGa_{1-x}As$ QD strain-engineered nanostructures.

In order to have a more general understanding of the dependence of the emission energy on the composition x of CLs and the QD-CL mismatch f, the dependence of the energy gap of the QD material (strained InAs), E_0^{QD}, and of the sum of band discontinuities on x and f has been calculated with our model and plotted in Fig. 8; the figure shows that the energy gap of the QD material, E_0^{QD}, is strongly dependent on the QD-CL mismatch f and then on the QD strain and changes little with the composition x, while the sum of the band discontinuities depends only on the CL composition x and is basically unaffected by the mismatch f. This observation substantiates the results shown in Fig. 4 and the comments made while discussing Fig. 6 as for the mechanisms that cause the redshift of the QD transitions.

These results can be qualitatively understood by simple arguments: (i) the dependence of the sum of the band discontinuities on x is due to the fact that only the energy gap of InGaAs CLs depends on x, while that of InAs QD is constant and (ii) its independence of f is related to the circumstance that both the energy gaps have a quite similar dependence on the mismatch. On the other hand, E_0^{QD} is almost constant with varying the composition of CLs at constant QD-CL mismatch, while it changes only with the QD strain determined by the QD-CL mismatch.

The slight dip in the QD energy gap for $x > 0.33$ stems from the change of the dependence of QD strain on QD-CL mismatch[40] that takes place when the QD morphology changes as a consequence of the increase of x. The reduced decrease of the sum of the band discontinuities is related to the slight decrease of E_0^{QD} as x increases that we have just discussed.

From all the above considerations, it follows that the ideas at the basis of the proposal of QD strain engineering[14,20] for tuning the QD emission energy in the windows of optoelectronic interest are confirmed by the experimental results and the model calculations in the structures considered. In addition, it is important to note that two independent parameters are available: the QD strain and the band discontinuities (through the QD-CL mismatch and the CL composition). Thanks to these two degrees of freedom, it is therefore possible to engineer two different characteristic quantities of QD structures. As it has been shown above one can be the emission wavelength, while the second can be chosen to be the activation energy for luminescence quenching, as discussed below.

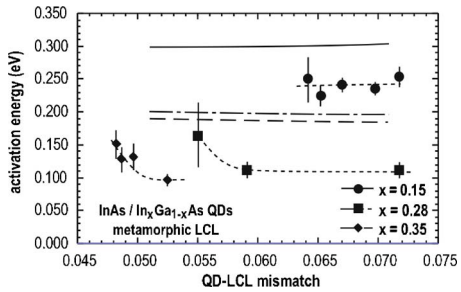

FIG. 9. Activation energy of thermal escape of carriers from QD states for $InAs/In_xGa_{1-x}As$ QD nanostructures on metamorphic LCLs. The dotted lines are guides for the eyes, while continuous, dashed, and dotted-dashed lines represent the results of model calculations.

D. Thermal quenching of photoluminescence

1. Activation energy of the quenching of luminescence

One of the most interesting properties for light-emitting devices is the luminescence efficiency at room temperature. The quenching of PL intensity with increasing temperatures is a quite general phenomenon that has been widely studied in the literature[49,50] and interpreted as due to the increased effectiveness of nonradiative mechanisms of confined carrier loss, in competition with radiative recombination. To study these processes in our strain-engineered structures we fitted the equation

$$I = \frac{I_0}{1 + a\exp(-E_1/kT) + b\exp(-E_2/kT)} \tag{2}$$

to the temperature (T) dependence of the integrated PL intensity I; the two exponential terms take into account two different processes with E_1 and E_2 activation energies.[20,51] As discussed in Refs. 49 and 50, the nonradiative process related to the largest activation energy is the confined carrier thermal escape from QD levels to CL or WL states. Since electrons and holes escape as correlated pairs,[49] the activation energy corresponds to the sum of the energy differences between CL or WL levels and QD ones both for electrons and holes. This conclusion was also arrived at in Ref. 50 where it was widely discussed that in a regime of low PL excitation with power densities below 10 W/cm^2 (such as the one under investigation here), the activation energy is equal to the total barrier height of electrons and holes, while it only corresponds to the barrier height of one type of carrier in a high excitation regime with power densities in the range of 100 W/cm^2. Therefore in our case this quantity is directly related to the sum of barriers for both carriers.

The values of the largest activation energy as deduced from the fitting of the Arrhenius plot of the integrated PL intensity for the $x=0.15$, 0.28, and 0.35 structures are plotted in Fig. 9 (symbols) as functions of the QD-CL mismatch. The values of the mismatch have been calculated with the procedure outlined in Sec. II B. In the same figure we plot the model calculations for the sum of the energy difference for both carriers between CL states and QD levels (lines) for

all the structures considered. From a comparison between the experimental activation energies and the model calculations it appears that the values predicted by the model fall consistently above the experimental values by several tens of meV (50–90 meV). This could be explained as due to approximations in the model or in the input parameters; alternatively we are led to conclude that the final states of the escape process are the WL states rather than CL ones,[49,20,52] that have energies a few tens of meV higher. The latter conclusion is supported by the photoreflectance results (Sec. III D 2) on the occurrence of transitions related to WL states at energies consistent with those obtained by the analysis of the thermal quenching of the photoluminescence intensity.

These considerations fully justify the idea that by using both QD-CL mismatch and CL composition as two independent parameters, the activation energy of PL can be optimized while keeping the emission energy at a given value.

By using our model, we may have a more quantitative insight on such an engineering process. In Fig. 7 the lower surface represents the sum of the electron and hole discontinuities that scales as the activation energy of the thermal escape of carriers from QDs. It can be noticed that when choosing (x,f) pairs on each one of the dashed lines on the (x,f) plane the emission wavelength is constant, while the activation energy can be maximized. To increase the activation energy of PL it is necessary to increase band discontinuities; the corresponding increase of confinement energies can be compensated for by decreasing the QD strain and then the band gap of the QD material.

As for the second contribution to the quenching process, with the smaller activation energy, we conclude that it is likely related to extrinsic processes connected to the presence of defects: (i) in the CLs, acting as traps for photogenerated carriers, with thermally activated capture cross section[53,54] and/or (ii) in proximity of the QDs, acting as channels for nonradiative recombination of carriers escaping from QDs.[51] Values of this activation energy as obtained by fitting the Arrhenius plots of the integrated PL intensities fall in the range of 30–70 meV; this range is consistent with the results of Ref. 51, where it was shown how the hydrogen irradiation is efficient in passivating nonradiative recombination channels.

2. Photoreflectance study of wetting layer states

The weak low energy PR feature (labeled E_{WL}) reported in Fig. 5 may be related to the optical response of the WL. As discussed above, to analyze these features we used the line shape given by Eq. (1) with $n=3$. For all structures with LCL composition $x=0.15$ the QW-like PR feature exhibited an energy typically smaller than the barrier band gap E_0^{HH} by 40–60 meV and an inhomogeneous broadening of 25–30 meV that is scarcely dependent on the temperature.

The evidence of the PR response from a WL associated with the growth of QD structures has been reported for InAs/GaAs QDs,[55] proving that the PR line shape maintains a two-dimensional (2D) excitonic character for InAs coverages up to 2 ML, although the QW-like spectral features broaden abruptly above 1.6 ML. Our present results are in agreement as regards the line shape broadening and the QW-like character with previous literature results,[28,56] confirming the occurrence of WL states in our structures. Considering that the oscillator strength of LH transitions in two-dimensional systems is three or two times less intense than that of HH ones (depending on whether the valence band mixing is considered),[57] we attribute the E_{WL} feature to the transition between electron and heavy-hole ground states in the InAs wetting layer.

It is interesting to note that the energy of WL states deduced by PR is in reasonable agreement with that of the final states of the thermal escape process that accounts for the thermal quenching of QD luminescence, as discussed in the previous section.

IV. CONCLUSIONS

In this paper we have thoroughly investigated the concept of quantum dot strain engineering that allows a few optical properties of QD nanostructures to be tailored using the QD strain as a parameter. A simple effective-mass model has been developed and used to analyze the experimentally determined optical properties of the structures.

We have shown that the strain of QDs can be effectively controlled not only by means of the CL composition, as it was already described in the literature, but also taking advantage of the thickness-dependent strain relaxation of LCLs that affects their lattice parameter. By means of strain, the energy gap of the QD material can be varied. On the other hand, the band discontinuities that confine the carriers into the QD volume can be determined by means of the composition of CLs. Therefore, by choosing the LCL thickness and the CL composition, the band discontinuities in the QD nanostructures and the energy gap of the QD materials can be predetermined and the emission energy can be tuned.

We note that the proposed approach yields two degrees of freedom that can be used to engineer both the emission energy and the activation energy for luminescence quenching at RT, a parameter that directly affects the RT emission efficiency. Our method has been experimentally proven and validated by means of model calculations, that have been shown to be sufficiently accurate for the design of the structures emitting at given wavelengths.

The structures have been grown by the combined use of MBE and ALMBE; the optical properties have been studied by photoluminescence and photoreflectance; in the latter case, advantage has been taken of the capability of PR of allowing the simultaneous investigation of transitions taking place in different constituents of the nanostructures, such as QDs, CLs, and WLs. The use of PL and PR has allowed the measurements of different relevant quantities of the structures, such as transition energies, band discontinuities, confinement energies, and activation counterparts for luminescence quenching.

It has been shown that the use of quantum dot strain engineering results in significant redshifts of the emission energy of InAs/InGaAs QD nanostructures and that emission wavelengths as long as 1.44 μm have been obtained at RT with excitation power densities as low as 5 W/cm^2.

It is worthwhile to notice that our approach is suffi-

ciently general so that it can be applied also to other material systems and that it can be used concomitantly with other methods that may result in a further increase of barriers confining the carriers in QDs.

Our results could open the way to the development of lasers for telecommunication applications operating at long wavelengths fabricated from nanostructures grown on GaAs substrates, a topic of huge technological interest. Such devices are predicted to have a relevant impact on the development of optoelectronic systems, since they could be very hardly realized on InP substrates and have several important advantages in comparison to the edge-emitting counterparts.

ACKNOWLEDGMENTS

This work has been partially supported by the MIUR-FIRB project "Nanotecnologie e Nanodispositivi per la Società dell'Informazione." The work at CNR-IMEM was partially carried out within the SANDiE Network of Excellence of EC, Contract No. NMP4-CT-2004-500101. The authors would like to acknowledge P. Allegri, V. Avanzini, and M. Bertocchi for valuable technical assistance. The AFM characterization has been carried out at CIM, University of Parma.

[1] D. Bimberg, M. Grundmann, and N. N. Ledentsov, *Quantum Dot Heterostructures* (Wiley, Chichester, 1999).
[2] M. S. Skolnick and D. J. Mowbray, Annu. Rev. Mater. Sci. **34**, 181 (2005).
[3] Y. Nakata, K. Mukai, N. Ohtsuka, M. Sugawara, H. Ishikawa, and N. Yokoyama, J. Cryst. Growth **208**, 93 (2000).
[4] M. J. da Silva, A. A. Quivy, S. Martini, T. E. Lamas, E. C. F. da Silva, and J. R. Leite, Appl. Phys. Lett. **82**, 2646 (2003).
[5] A. Bosacchi, P. Frigeri, S. Franchi, P. Allegri, and V. Avanzini, J. Cryst. Growth **175/176**, 771 (1997).
[6] K. Mukai, N. Ohtsuka, M. Sugawara, and S. Yamazaki, Jpn. J. Appl. Phys., Part 2 **33**, L1710 (1994).
[7] R. P. Mirin, J. P. Ibbetson, K. Nishi, A. C. Gossard, and J. E. Bowers, Appl. Phys. Lett. **67**, 3795 (1995).
[8] F. Guffarth, R. Heitz, A. Schliwa, O. Stier, N. N. Ledentsov, A. R. Kovsh, V. M. Ustinov, and D. Bimberg, Phys. Rev. B **64**, 085305 (2001).
[9] K. Nishi, H. Saito, S. Sugou, and J. Lee, Appl. Phys. Lett. **74**, 1111 (1999).
[10] J. X. Chen *et al.*, J. Appl. Phys. **91**, 6710 (2002).
[11] H. Y. Liu, I. R. Sellers, M. Hopkinson, C. N. Harrison, D. J. Mowbray, and M. S. Skolnick, Appl. Phys. Lett. **83**, 3716 (2003).
[12] F. Ferdos, M. Sadeghi, Q. X. Zhao, S. M. Wang, and A. Larsson, J. Cryst. Growth **227–228**, 1140 (2001).
[13] M. V. Maximov *et al.*, Phys. Rev. B **62**, 16671 (2000).
[14] L. Seravalli, M. Minelli, P. Frigeri, P. Allegri, V. Avanzini, and S. Franchi, Appl. Phys. Lett. **82**, 2341 (2003).
[15] Y. C. Xin, L. G. Vaughn, L. R. Dawson, A. Stintz, Y. Lin, L. F. Lester, and D. L. Huffaker, J. Appl. Phys. **94**, 2133 (2003).
[16] L. Ya. Karachinsky *et al.*, Semiconductors **39**, 1415 (2005).
[17] K. Nishi, M. Yamada, T. Anan, A. Gomyo, and S. Sugou, Appl. Phys. Lett. **73**, 526 (1998); A. E. Zhukov *et al.*, Semiconductors **32**, 795 (1998).
[18] M. Geddo *et al.*, in *Nanoscale Devices, Materials, and Biological Systems: Fundamental and Applications*, edited by M. Cahay, S. Bandyopadhyay, H. Hasegawa, J. P. Leburton, S. Seal, M. Urquidi-Macdonald, P. Guo, N. Koshida, D. J. Lockwood, and A. Stella (Electrochemical Society, Pennington, NJ, 2005), Vol. 13, p. 373.
[19] M. Geddo, G. Guizzetti, M. Patrini, T. Ciabattoni, L. Seravalli, P. Frigeri, and S. Franchi, Appl. Phys. Lett. **87**, 263120 (2005).
[20] L. Seravalli, M. Minelli, P. Frigeri, P. Allegri, V. Avanzini, and S. Franchi, Appl. Phys. Lett. **87**, 063101 (2005).
[21] ALMBE is a variant of MBE where group-III and group-V species impinge on the substrate alternatively in monolayer or submonolayer amounts per cycle. F. Briones and A. Ruiz, J. Cryst. Growth **111**, 194 (1991).
[22] D. E. Aspnes, Surf. Sci. **37**, 418 (1973).
[23] H. Shen, S. H. Panad, and F. H. Pollak, Phys. Rev. B **37**, 10919 (1988).
[24] J. Glembocki and B. Shanabrook, in *The Spectroscopy of Semiconductors*, Semiconductors and Semimetals Vol. 36, edited by D. G. Seiler and C. L. Littler (Academic, Boston, 1992), p. 221.
[25] L. Aigouy, T. Holden, F. H. Pollak, N. N. Ledentsov, W. M. Ustinov, P. S. Kop'ev, and D. Bimberg, Appl. Phys. Lett. **70**, 3329 (1997).
[26] F. H. Pollak, in *Handbook on Semiconductors*, edited by P. Balkansky (North-Holland, Amsterdam, 1994), Vol. 52, p. 527.
[27] G. L. Rowland, T. J. C. Hosea, S. Malik, D. Childs, and R. Murray, Appl. Phys. Lett. **73**, 3268 (1998).
[28] M. Geddo, R. Ferrini, G. Guizzetti, M. Patrini, S. Franchi, P. Frigeri, G. Salviati, and L. Lazzarini, Eur. Phys. J. B **16**, 19 (2000).
[29] P. M. J. Marée, J. C. Barbour, J. F. Van der Veen, K. L. Kavanagh, C. W. T. Bulle-Lieuwma, and M. P. A. Viegers, J. Appl. Phys. **62**, 4413 (1987).
[30] J. W. Matthews and A. E. Blakeslee, J. Cryst. Growth **27**, 118 (1974).
[31] D. J. Dunstan, P. Kidd, L. K. Howard, and R. P. Dixon, Appl. Phys. Lett. **59**, 3390 (1991).
[32] J. Y. Marzin and G. Bastard, Solid State Commun. **92**, 437 (1994).
[33] A. J. Williamson, L. W. Wang, and A. Zunger, Phys. Rev. B **62**, 12963 (2000).
[34] M. Grundmann, O. Stier, and D. Bimberg, Phys. Rev. B **52**, 11969 (1995).
[35] M. A. Cusack, P. R. Briddon, and M. Jaros, Phys. Rev. B **54**, R2300 (1996).
[36] H. Jiang and J. Singh, Phys. Rev. B **56**, 4696 (1997).
[37] G. Cipriani, M. Rosa-Clot, and S. Taddei, Phys. Rev. B **62**, 4413 (2000).
[38] D. M. Bruls *et al.*, Appl. Phys. Lett. **81**, 1708 (2002).
[39] Q. Gong, P. Offermans, R. Notzel, P. M. Koenraad, and J. H. Wolter, Appl. Phys. Lett. **85**, 5697 (2004).
[40] A. D. Andreev, J. R. Downes, D. A. Faux, and E. P. O'Reilly, J. Appl. Phys. **86**, 297 (1999).
[41] C. G. Van de Walle, Phys. Rev. B **39**, 1871 (1989).
[42] M. Cardona and N. E. Christensen, Phys. Rev. B **37**, 1011 (1988).
[43] I. Vurgaftman, J. R. Meyer, and L. R. Ram-Mohan, J. Appl. Phys. **89**, 5815 (2001).
[44] Y. P. Varshni, Physica (Utrecht) **34**, 149 (1967).
[45] S. Adachi, J. Appl. Phys. **53**, 8775 (1982).
[46] J. Singh, in *Properties of Lattice-Matched and Strained Indium Gallium Arsenide*, edited by P. Bhatthacharya (Inspec, London, 1993), p. 61.
[47] F. H. Pollak and M. Cardona, Phys. Rev. B **172**, 816 (1968).
[48] F. H. Pollak, in *Strained-Layer Superlattices: Physics*, Semiconductors and Semimetals Vol. 32, edited by T. P. Pearsall (Academic, London, 1990), p. 17.
[49] S. Sanguinetti, M. Henini, M. Grassi Alessi, M. Capizzi, P. Frigeri, and S. Franchi, Phys. Rev. B **60**, 8276 (1999).
[50] E. C. Le Ru, J. Fack, and R. Murray, Phys. Rev. B **67**, 245318 (2003).
[51] S. Mazzucato, D. Nardin, M. Capizzi, A. Polimeni, A. Frova, P. Frigeri, L. Seravalli, and S. Franchi, Mater. Sci. Eng., C **25**, 830 (2005).
[52] L. Seravalli, M. Minelli, P. Frigeri, P. Allegri, V. Avanzini, and S. Franchi, Mater. Sci. Eng., C **26**, 731 (2006).
[53] D. Colombo *et al.*, J. Appl. Phys. **94**, 6513 (2003).
[54] K. Mukai, N. Ohtsuka, and M. Sugawara, Appl. Phys. Lett. **70**, 2416 (1997).
[55] M. Geddo, M. Capizzi, A. Patanè, and F. Martelli, J. Appl. Phys. **84**, 3374 (1998).
[56] W. Rudno-Rudzinski *et al.*, Appl. Phys. Lett. **86**, 101904 (2005).
[57] L. C. Andreani and A. Pasquarello, Phys. Rev. B **42**, 8928 (1990).